Supporting Information: Experimental setup and approach, data analysis, position lock technique, Mie theory, FDTD simulations and analytical derivations

A. A. P. Trichet *[1], P. R. Dolan[1], D. James[2], G. M. Hughes[1], C. Vallance[2], and J. M. Smith[1]

[1]Department of Materials, University of Oxford, OX1 3PH, UK
[2]Department of Chemistry, University of Oxford, OX1 3RQ, UK

September 14, 2016

Microcavity chip and optical setup

The microcavities are situated on a chip which is 300 µm × 300 µm as shown in Figure S1 a). During an experiment, we can address microcavities with different RoC's as well as identical ones. The red laser is split into two spots, one for the reference cavity (dashed white circle in Figure S1 a)), the other for the trapping one (blue circle in Figure S1 a)).

Figure S1 b) is a scheme of the flow cell and optical setup described in the Methods section of the main paper. The green laser, at the edge of the stop band, is used to stabilize and position the microcavities down to ≈ 100 pm via a feedback loop with a 50 Hz refresh rate. The red laser probes the microcavities transmission while the cavity length is scanned at 5 kHz.

Effect of the scanning mirror on the nanoparticle movement

In this work, the cavity length is scanned over 1.2 nm for a mirror separation of 960 nm, ie. a 0.13% change in cavity length. Based on these numbers, it is reasonable to assume that the cavity length modulation is not affecting the longitudinal movement of the nanoparticle.

Since water is incompressible and that the water can freely move in and out of the intra-mirror space, the length change can indeed produce a transverse movement for the liquid. This movement depends on the microcavity position with respect to the centre of the 300 µm x 300 µm chip. The microcavity used for this experiment is situated at 18 µm from the centre of the chip. Using a volume conservation considerations, one can derive the following equation: $dR = R_0 \left[\sqrt{\frac{L_0}{L_0 - dL}} - 1\right]$ where R_0 is the distance of the microcavity to the distance of the chip ($R_0 = 18\,\mu$m for the data presented in this work), $L_0 = 400$ nm is the flat mirror separation and dL is the scanning length. For the microcavity used for this experiment, the cavity length change corresponds to a liquid transverse movement of 27 nm. This value is much smaller than the characteristic transverse parameters of the microcavity mode.

Additionally, if the mirror scanning was disturbing the nanoparticle movement, we would observe non-Lorentzian lineshapes, oscillating signal in the mode shift as well as non-exponential decay in the autocorrelation function.

Overall, we can safely assume that the disturbance to the nanoparticle movement by the scanning mirror is negligible and does not affect our results.

Data analysis and calibration

The output of the oscilloscope is a file containing 5 millions of points and giving the APD voltage as a function of time. Each scan is stacked one on top of the other. At 5 kHz, the response of the DC piezoelectric stack cannot be assumed to follow the input voltage accurately without a phase delay. Therefore, we cannot use the voltage signal to un-

*aurelien.trichet@materials.ox.ac.uk

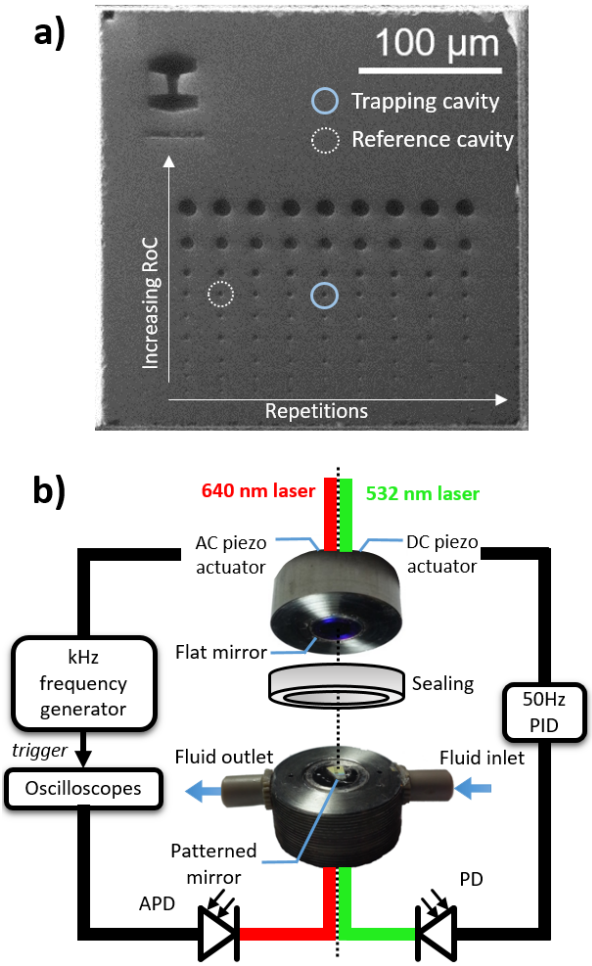


Figure S 1: a) SEM image of the chip template displaying different RoC microcavities (vertical axis) and repetitions (horizontal axis). The trapping and reference cavities are exemplified, respectively, with a blue plain and white dashed circles. b) Exploded view of the flow cell embedded in the scanning (left, red laser) and stabilization feedback (right, green laser) loops

wrap and calibrate the signal. Instead, we perform an autocorrelation of the signal to find its period and an anti-correlation to find the start of the first period. The scans can then be stacked upon one another to form an uncalibrated version of figure 2 b) in the main paper.

In order to calibrate these images, we use our red laser in a multimode regime and measure its splitting with a wavemeter (WS6 from High Finesse) leading to a value of 26 pm. The transmission of a single empty cavity is then recorded in real-time while the mode is moved across the scanning range. Consequently, we can attach a wavelength splitting for each point of the scanning window giving us our spectrum calibration. The uncalibrated images are then interpolated using this calibration run with the same number of points. This calibration is performed for every experimental run to avoid artefacts.

Each spectrum is fitted using a double Lorentzian function in Matlab. Since our time resolution is smaller than the mode shift characteristic times, we use the parameters obtained for a scan on the next one. As an example, the treatment of the event presented on figure 2 b) in the main paper requires 25000 consecutive fits. Thanks to the error bars and goodness of fit parameters, we can eliminate points with poor fits for figures 4 b) and 5 b) in the main paper.

Position lock-in of the mirrors

In order to control and lock the mirror in position, we use a custom control and lock system coupled to a feedback loop (see Figure S1 b)). A green laser is split into two beams and focused on two different positions on the plinth. Each of the transmitted intensities is collected onto a different photodiode and acquired on a data acquisition card. The normalized transmitted intensities I_1 and I_2 at a wavelength λ_g = 532 nm in water (n = 1.33) can be approximated by:

$$I_1 = cos\left(\frac{2\pi nL}{\lambda_g}\right) \tag{1}$$

$$I_2 = cos\left(\frac{2\pi nL}{\lambda_g} + \delta\right) \tag{2}$$

where L is the cavity length and δ is a phase difference term between the two transmitted beams. We can freely change the phase term δ using the set of kinematics on the mirror holders and we tune it to be $\delta = \frac{\pi}{2}$. We can then compute the Lissajous-like expression:

$$\widetilde{I} = I_1 + iI_2 = e^{-\frac{2i\pi nL}{\lambda_g}} \tag{3}$$

In the complex plane, $\widetilde{I}$ corresponds to a point moving on a quasi-circular shape. By simply tracking the phase of this parameter, one can read the relative length change over more than one loop, ie. for $\Delta L = \lambda_g/2n$. The length reader is initialized by

bringing the two mirrors into contact prior to starting the trapping sequence. This tool is crucial in order to properly track the same optical mode over the entire experiment.

Once the length is being read in real-time, we use a LabVIEW program to calculate a feedback voltage that is applied to the DC piezo-electric stack controlling the cavity length. Using this method, we obtain a positioning accuracy of around 10 pm with a 50 Hz refresh rate, mainly limited by the computer speed and voltage source accuracy.

Thermal bistability

Microcavities generally display thermal bistability behaviour for high intra-cavity power. We do observe this effect for low scanning frequency for the AC piezoelectric stack below ≈ 500 Hz. However, at higher frequencies, pure Lorentzian lineshapes are recovered due to a frequency cut-off of the DBR heating well below our scanning frequency. Therefore, cavity heating can be considered to be an averaged effect over the course of the experiment rather than dynamic heating from a single scan.

Mie theory and FDTD simulations

Mie theory

The Mie theory calculations were performed using the optical tweezers computational toolbox [1]. The beam waist choosen for this simulation is matched onto the FDTD simulations. Two counter-propagating wave where superimposed in order to form a standing wave. The base states number used was 41, based on prior convergence tests. The toolbox gives access to the transverse trapping efficiency of the system $Q_{x,y}$. This parameter is proportional to the polarizability of the nanoparticle. The toolbox is therefore used to compute the trapping efficiency $Q_{x,y}$ as a function of the nanoparticle radius and the results are normalized to the dipole model for small radii. To create the potential maps, we compute the longitudinal and transverse trapping efficiency Q_z and $Q_{x,y}$ for a single nanoparticle radius for each position in the mode wavefunction. Since the trapping efficiency is proportional to the trapping force, we can integrate Q_z and $Q_{x,y}$ to obtain the normalized potential map.

Averaged dipole theory

Within the averaged dipole theory, we assume that the nanoparticle response to an electromagnetic excitation is given by integrating the response of a infinitely small single dipole over the full nanoparticle volume. Therefore, this model takes into account the finite size of our nanoparticle but neglects the Mie resonances taking place. In this calculation, we use the Gaussian beam framework to model the mode wavefunction $\widetilde{I}$ and the waist is matched to the FDTD simulations. The averaged polarizability α_{avg} is then given by:

$$\alpha_{avg} = \alpha \iiint_{V_{NP}} \widetilde{I} \, \frac{dV}{V_{NP}} \tag{4}$$

where V_{NP} is the nanoparticle volume. The integral is performed for a particle at the maximum of the field. Notice that in this expression, the mode wavefunction $\widetilde{I}$ is normalized to the intensity at the anti-node and is dimensionless. We compute this integral after analytical simplification in Matlab.

FDTD simulations

To obtain accurate estimates for the volume of the cavity modes, finite difference time domain (FDTD) simulations were performed with "Lumerical", a commercially available software package. These simulations consisted of a full 3 dimensional reconstruction of the cavity making use of specific topographical information taken from the FIB milling construction routine. A broadband dipole source was used to excite all of the resonances present in the structure, and the field distribution corresponding to the relevant TEM00 mode was selected from a power monitor, which integrates and stores field contributions from a pre-defined spectral range. This cross sectional field distribution was normalised and integrated, exploiting the mode's cylindrical symmetry to yield the corresponding volume.

It should be noted that Finite Difference Time Domain (FDTD) is not directly suited to measure small mode linewidth changes and small shifts for such high-Q microcavities. Simulation time would exceed couple of weeks on a dedicated supercomputer to have a sufficient resolution. However, we can demonstrate that the density of states can be reduced in a microcavity by comparing the power monitors for a nanoparticle immersed in water with

and without a microcavity around it. To evaluate the effect of the cavity on the scattering by a nanoparticle located at a field antinode, a dipole source was placed at the centre of the sphere. By monitoring the dipole power of the injected field, the spectral Purcell factor for both cases (with and without cavity) can ascertained. The Purcell factor for the case without a cavity present can then be used to normalise the enhancement factor observed with the cavity included, and therefore show the role that the cavity plays in altering the available density of states. The results of this analysis is displayed in the following figure. The ratio obtained with FDTD $\frac{\rho_c}{\rho_{fs}}$ can be expressed as follow: $\frac{\rho_c}{\rho_{fs}} = \beta_{fs} + F_P$ where F_P is the Purcell factor and β_{fs} is the coupling to free-space. Generally, β_{fs} is assumed to be unity for large cavities with sufficient access to free-space. In the case of figure 3 b), we are only interested to this last parameter since the nanoparticle is not an emitter. Consequently, in the simulation, we have detuned the mode from 640 nm in order to observe the free-space coupled at this wavelength. We obtained a reduction of the available density of states of 60%, in excellent agreement with the measured value estimated around 65%.

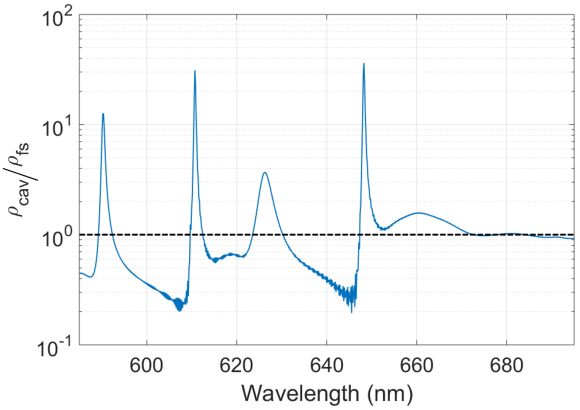


Figure S 2: Normalized available density of states for a 200nm nanoparticle in a microcavity

Trap density of states calculation

The DoS of the trap can be computed using either the FDTD simulation or the effective polarizability map in Mie theory. The number of positions for each intensity are counted including the cylindrical symmetry leading directly to the DoS.

Trapping potential energy and link with the parabolic approximation

The potential energy U associated with the optical trap is given by:

$$U = -\frac{\alpha}{n_w c \epsilon_0} I_0 \widetilde{I}(r) \tag{5}$$

and is maximum for $\widetilde{I}(r) = 1$, ie. when the particle is at the maximum of the electromagnetic field. We use here the Gaussian beam framework within the paraxial approximation to model the mode wavefunction. In our system, the cavity modes are clearly out of the paraxial approximation, however, this model gives us a direct way to express the spring constant of the trap and only a small deviation with the FDTD case is expected here, especially for the longitudinal spring constant. In this case, the normalized intensity of the mode can be written:

$$\widetilde{I}(r) = cos^2\left(\frac{2\pi z}{(\lambda/n_w)}\right) \times e^{-\frac{2\left(x^2+y^2\right)}{\omega_0^2}} \tag{6}$$

and can be approximated, close to the bottom of the trap by:

$$\widetilde{I}(r) = \left[1 - \left(\frac{2\pi}{(\lambda/n_w)}\right)^2 z^2\right] \times \left[1 - \frac{2}{\omega_0^2}\left(x^2+y^2\right)\right] \tag{7}$$

We can therefore compute the longitudinal and transverse spring constants k_z and $k_{x,y}$:

$$k_{x,y} = \frac{\alpha}{n_w c \epsilon_0} I_0 \frac{4}{\omega_0^2} \tag{8}$$

$$k_z = \frac{2\alpha}{n_w c \epsilon_0} I_0 \left(\frac{2\pi}{(\lambda/n_w)}\right)^2 \tag{9}$$

where ω_0 is the waist of the cavity mode obtained from FDTD.

Derivation of the Boltzmann factor in the PO

In order to derive the Boltzmann factor in the PO, we can use an alternative form of equation 5 given by:

$$U = -\frac{\alpha}{n_w c \epsilon_0} I_0 \Delta\widetilde{\lambda} \tag{10}$$

Therefore, if we start with the usual Boltzmann distribution f_B in energy:

$$f_B(U) = \frac{1}{k_B T} e^{-\frac{U}{k_b T}} \tag{11}$$

and we use the relation:

$$f_B(U)dU = f_B(\Delta\widetilde{\lambda})d\Delta\widetilde{\lambda} \tag{12}$$

we can write the Boltzmann factor $f_B(\Delta\lambda)$ in terms of wavelength shift such as:

$$f_B(\Delta\widetilde{\lambda}) = -fe^{-f\left[1-\Delta\widetilde{\lambda}\right]} \tag{13}$$

where:

$$f = \frac{\alpha}{n_w c\epsilon_0}\frac{I_0}{k_B T} \tag{14}$$

Derivation of the autocorrelation function of the mode shift

In this section, we compute the autocorrelation function of the mode shift within the parabolic approximation. In order to do so, we use first an analytical equation based on numerical Monte Carlo simulations. Then, we derive the complete autocorrelation function and verify the results with a second set of Monte Carlo simulations.

Preamble

First of all, we want to establish the analytical expression for the autocorrelation of the squared position $\mathcal{C}_{x^2}$ of a particle trapped in a harmonic trap. We aim to show that:

$$\mathcal{C}_{x^2} = \mathcal{C}_x^2 = \left(e^{-\frac{k\tau}{\gamma}}\right)^2 \tag{15}$$

In the general case, this relation is mathematically wrong. However, we can show numerically that it is satisfied for Brownian motion in a parabolic trap using a Monte Carlo simulation.

We use a Matlab program that simulates the trajectory of a particle undergoing Brownian motion in an optical trap based on reference [2]. All the parameters used in this simulation are similar to the one presented in the paper (particle size, spring constants, etc...). Each particle position is associated with a normalized mode shift via the parabolic wavefunction. For each realization of the particle trajectory, we compute the autocorrelation of the mode shift and perform an exponential fit as shown in Figure S3 a). The spring constants are then swept within the range [1 % - 110 %] in order to cover the spring constants observed in our experimental work. For each set of parameters, the results are averaged over 30 realizations. The time constants obtained are displayed in Figure S3. The black line corresponds to the theoretical expectations based on equation 15 and leads to an excellent fit. As a conclusion, we can therefore confidently use the assumption: $\mathcal{C}_{x^2} = \mathcal{C}_x^2$ for the system considered in this work.

Derivation

Firstly we compute the mean mode normalized shift:

$$\mu_{\Delta\widetilde{\lambda}} = \left\langle \widetilde{I}(r) \right\rangle \tag{16}$$

Since $\left\langle z^2 \right\rangle = \frac{k_B T}{k_z}$ and $\left\langle (x^2+y^2) \right\rangle = \frac{2k_B T}{k_{x,y}}$, by neglecting the higher order terms, we obtain:

$$\mu_{\Delta\widetilde{\lambda}} = \left(1 - \frac{3}{2}f\right) \tag{17}$$

The autocorrelation function of the normalized mode shift can be written:

$$\mathcal{C}_{\Delta\widetilde{\lambda}} \propto \left\langle \left(\Delta\widetilde{\lambda}(t) - \mu_{\Delta\widetilde{\lambda}}\right)\left(\Delta\widetilde{\lambda}(t+\tau) - \mu_{\Delta\widetilde{\lambda}}\right) \right\rangle \tag{18}$$

Using equations 7 and 16, neglecting the higher order terms and normalizing, we obtain:

$$\mathcal{C}_{\Delta\widetilde{\lambda}} \propto \left[k_z \mathcal{C}_{z^2} + k_{x,y}\mathcal{C}_{x^2+y^2}\right] \tag{19}$$

One can show that $\mathcal{C}_{x^2+y^2} = 2\mathcal{C}_{x^2}$. Using the relations established earlier such as $\mathcal{C}_{z^2} = (\mathcal{C}_z)^2$, we finally derive:

$$\mathcal{C}_{\Delta\widetilde{\lambda}} = \left[\frac{1}{3}e^{-\frac{\tau}{\tau_z}} + \frac{2}{3}e^{-\frac{\tau}{\tau_{x,y}}}\right] \tag{20}$$

where $\tau_z = \frac{\gamma_z}{2k_z}$ and $\tau_{x,y} = \frac{\gamma_{x,y}}{2k_{x,y}}$.

Numerical Monte Carlo simulation

In order to confirm the validity of equation 20 for our trap, we performed Monte Carlo simulations to test it. These simulations are based on the same principle as the one developed in the preamble of this derivation. However, the trap is taken to be anisotropic here according to the experiment.

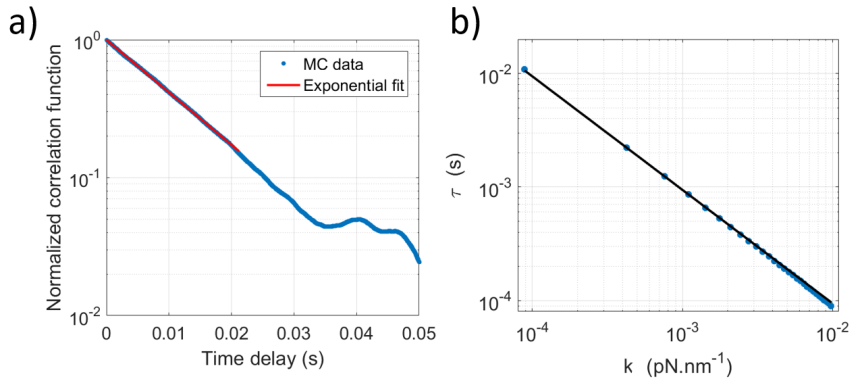


Figure S 3: Monte Carlo simulation of an isotropic trap. a) Normalized autocorrelation function of the mode shift for a single realization. Blue dots: Monte Carlo simulation. Red line: exponential fit. b) Correlation time constants τ as a function of the spring constant k. Black line: theoretical expectations

For each realization, we compute the autocorrelation of the mode shift and performed a fit of equation 20 with the two time constants τ_z and $\tau_{x,y}$ as well as the dimensionality factor as free parameters. The result of the fit for a single realization is shown on Figure S4 a). The spring constants are then swept within the range [40 % - 110 %] of their maximal value in the experiment. For each point, the simulation is repeated 30 times and the results are averaged over these realizations. The time constants obtained are displayed in Figures S4 b) and c). The black line corresponds to the theoretical expectations and gives an excellent fit. As shown on Figure S4 d), the dimensionality factor of $\frac{1}{3}$ is recovered for the mode shift autocorrelation. In conclusion, we can therefore confidently apply equation 20 to the mode shift data within the parabolic approximation.

Effective spring constants calculation

In order to estimate the equivalent spring constant of our system despite its anharmonicity, we use the FDTD simulation of the trap along with the equipartition theorem.

For the z-direction, the equipartition theorem reads:

$$\frac{1}{2}\langle k_z\rangle\langle z^2\rangle = \frac{1}{2}k_BT \tag{21}$$

which can be re-arranged to obtain the effective spring constant:

$$\langle k_z\rangle = \frac{k_BT}{\langle z^2\rangle} \tag{22}$$

where $\langle z^2\rangle$ is computed using the Boltzmann factor and the measurement of the trap strength such as:

$$\langle z^2\rangle = \frac{1}{2}\int_1^0 z^2(\Delta\widetilde{\lambda})f_B(\Delta\widetilde{\lambda})d\Delta\widetilde{\lambda} \tag{23}$$

where:

$$f_B(\Delta\widetilde{\lambda}) = -fe^{-f[1-\Delta\widetilde{\lambda}]} \tag{24}$$

The term $z^2(\Delta\widetilde{\lambda})$ is computed using the FDTD simulation of the mode wavefunction. Same calculations are applied along the transverse directions x and y.

References

[1] Timo A Nieminen, Vincent LY Loke, Alexander B Stilgoe, Gregor Knöner, Agata M Brańczyk, Norman R Heckenberg, and Halina Rubinsztein-Dunlop. Optical tweezers computational toolbox. *Journal of Optics A: Pure and Applied Optics*, 9(8):S196, 2007.

[2] Giorgio Volpe and Giovanni Volpe. Simulation of a brownian particle in an optical trap. *American Journal of Physics*, 81(3):224–230, 2013.

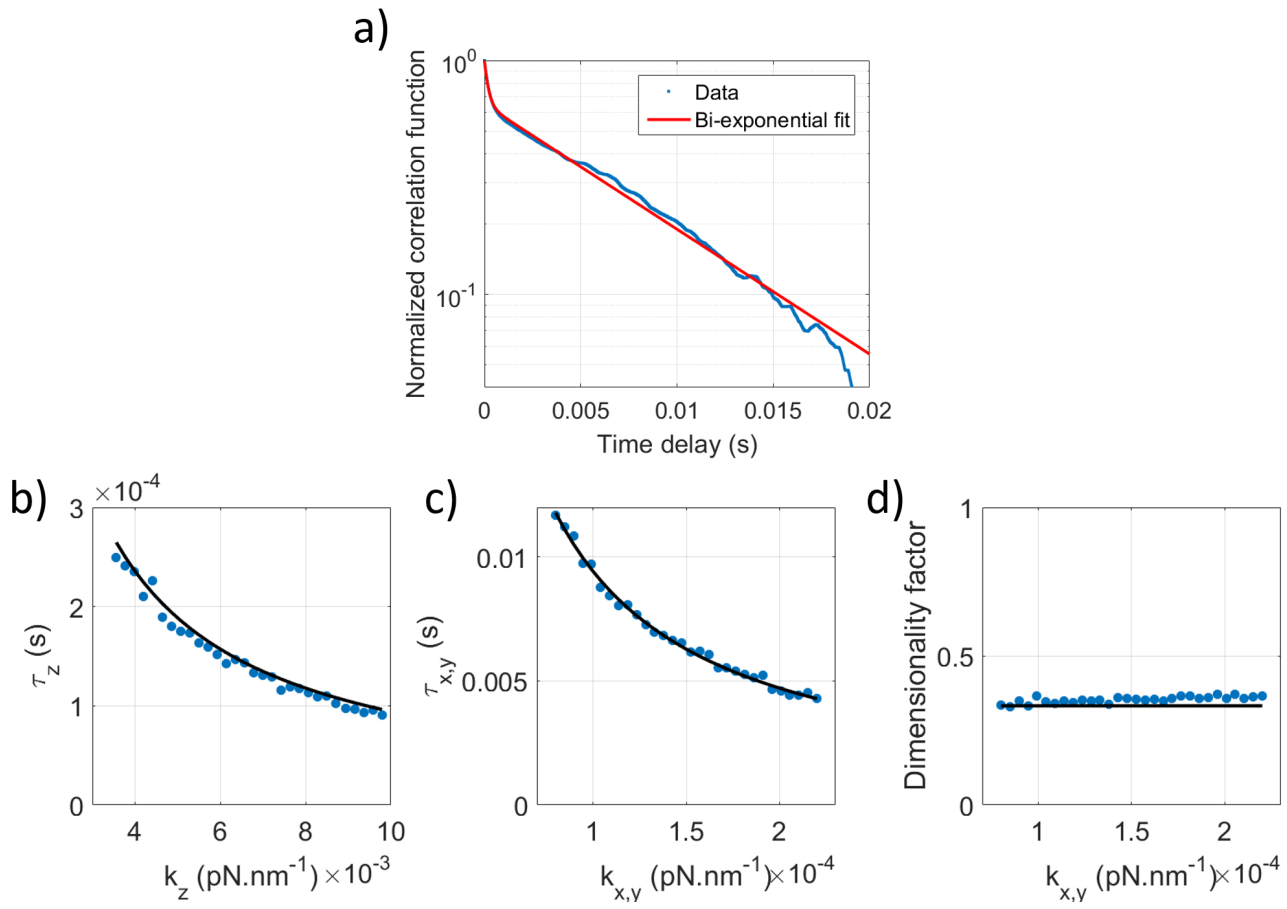


Figure S 4: Monte Carlo simulation of an anisotropic trap. a) Normalized autocorrelation function of the mode shift for a single realization. Blue dots: Monte Carlo simulation. Red line: bi-exponential fit. b) and c) Correlation time constants τ_z (left) and $\tau_{x,y}$ (middle) as a function of the spring constant k_z and $k_{x,y}$. Black line: theoretical expectations d) Dimensionality factor x as function of the transverse spring constant $k_{x,y}$ (blue dots). Black dashed line: Theoretical expectation